NASA

Technical Memorandum 84934

THE UTILIZATION OF NIMBUS-7 SMMR MEASUREMENTS TO DELINEATE RAINFALL OVER LAND

Edward Rogers and Honnappa Siddalingaiah

NOVEMBER 1982

National Aeronautics and
Space Administration

Goddard Space Flight Center
Greenbelt, Maryland 20771

NASA TECHNICAL MEMORANDUM

The Utilization of Nimbus-7 SMMR Measurements to Delineate Rainfall Overland

by

Edward Rodgers[1] and Honnappa Siddalingaiah[2]

[1]Goddard Laboratory for Atmospheric Sciences (GLAS) NASA/Goddard Space Flight Center, Greenbelt, Maryland 20771.

[2]OAO Corporation, Greenbelt, Maryland 20770.

November 1982
NASA/Goddard Space Flight Center

TABLE OF CONTENTS

		Page
	Abstract	x
1	Introduction	1
2	The SMMR System	7
3	Data Sampling	9
4	Statistical Analysis	19
5	Classification Algorithm	31
6	Error Analysis	35
7	Algorithm Evaluation	41
8	Conclusion and Recommendations	49
	References	53

FIGURES

Figure		Page
1	Rain rate versus T_B (°K)	2
2	Lake Charles LA area, 30 May 1979, remapped GOES-1 IR data	11
3	Lake Charles LA area, 30 May 1979, remapped WSR 57 Radar PPI data	12
4	Lake Charles LA area, 30 May 1979, remapped Nimbus-7 SMMR vertically polarized 37.0 GHz data	13
5	Miami FL Area, 3 September 1979, Remapped GOES-1 IR data	15
6	Miami FL, 3 September 1979, Remapped WSR 57 Radar PPI Data	16
7	Miami FL Area, 3 September 1979, Remapped Nimbus-7 SMMR vertically polarized 37.0 GHz data	17
8	Nimbus-7 SMMR 37.0 GHz channel scatter-plots for T_H versus T_V	23
9	Nimbus-7 SMMR 18.0 GHz channel scatter-plots for T_H versus T_V	24
10	Nimbus-7 SMMR 10.7 GHz channel scatter-plots for T_H versus T_V	25
11	Centerville AL, 11 July 1979, remapped WSR 57 Radar PPI data	38
12	Centerville AL Area, 11 July 1979, hourly rainfall data	39
13	Centerville AL Area, 11 July 1979, remapped GOES-1 IR data	42
14	Centerville AL Area, 11 July 1979, rain locations from Nimbus-7 SMMR 37.0 GHz data	43
15	Centerville AL Area, 11 July 1979, rain locations from Nimbus-7 SMMR 18.0 GHz data	44
16	Centerville AL Area, 11 July 1979, rain locations from Nimbus-7 SMMR 10.0 GHz data	45

TABLES

Table		Page
1	Dates of Rain Cases	10
2	Elementary Statistics of Samples 37 GHz Data	20
3	Elementary Statistics of Sampled 18 GHz Data	21
4	Elementary Statistics of Sampled 10.6 GHz Data	22
5	Significance Between Means (F Test) SMMR 37 GHz Channel	27
6	Significance Between Means (F Test) SMMR 18 GHz Channel	28
7	Significance Between Means (F Test) SMMR 10 GHz Channel	28
8	Probability of Misclassification: Theoretical Computation SMMR 37 GHz Channel	36
9	Probability of Misclassification Theoretical Computation SMMR 18 GHz Channel	36
10	Probability of Misclassification Theoretical Computation SMMR 10 GHz Channel	37

The Utilization of Nimbus 7 SMMR Measurements to Delineate Rainfall Over Land

Edward Rodgers[1]

Honnappa Siddalingaiah[2]

ABSTRACT

Based on previous theoretical calculations, an empirical statistical approach to use satellite multifrequency dual polarized passive microwave data to detect rainfall areas over land was initiated. The addition of information from a lower frequency channel (18.0 or 10.7 GHz) was shown to improve the discrimination of rain from wet ground achieved by using a single frequency dual polarized (37 GHz) channel alone.

The algorithm was developed and independently tested using data from the Nimbus-7 Scanning Multichannel Microwave Radiometer (SMMR). Horizontally and vertically polarized brightness temperature pairs (T_H, T_V) at 37, 18, 10.7 GHz were sampled for raining areas over land (determined from ground base radar), wet ground areas (adjacent and upwind from rain areas determined from radar), and dry land regions (areas where rain had not fallen in a 24h period) over the central and eastern United States. Surface thermodynamic temperatures were both above and below 15°C. An examination of the data from each separate channel indicated that the probability (using the F test) that the mean vectors of any two populations being identical is less than .01 for classes sampled with surface thermodynamic temperatures $\geq$ 15°C except

---

[1]Laboratory for Atmospheric Sciences (GLAS), Goddard Space Flight Center/NASA, Greenbelt, MD 20771

[2]OAO Corporation, Greenbelt, MD 20770

for the rain over land and wet ground classes observed with the SMMR 37 GHz channel. For the classes sampled with surface thermodynamic temperatures < 15°C, none of the classes were significantly different.

Since most of the categories were significantly different for the warmer ($\geq$15°C) land surface cases, a Fisher linear discriminant classifier was then developed for each channel and independently tested. The results from one test case showed that for areas of large scale heavy rainfall, the lower frequency SMMR channels were better able to delineate rain from wet ground than the 37 GHz channel. However, in areas of light rain and/or where the rain area did not fill the lower frequency instantaneous field of view these channels were not able to differentiate rain from wet ground.

The Utilization of Nimbus 7 SMMR Measurements to Delineate Rainfall Over Land

1. INTRODUCTION

Theoretical calculations (Savage and Weinman, 1975; Savage et al., 1976[1]; and Wienman and Guetter, 1977) have indicated that at 37 GHz rainfall could be detected over land surfaces. These results showed that at 37 GHz and at a viewing angle of 50° from nadir the radiance emerging from hydrometeors is relatively small (due to scattering) and unpolarized; while radiance emerging from wet land surfaces is also relatively small but polarized; and radiance emerging from dry land surfaces is relatively large. These results were partially verified empirically by Rodgers et al., (1979) by comparing large scale rainfall over land utilizing the Nimbus-6 Electrically Scanning Microwave Radiometer (ESMR-6) data. The study showed that large scale rainfall over land, where surface thermodynamic temperatures were greater than 15°C and where the vegetation was not covered with dew, could be delineated from dry land surfaces despite the large ESMR-6 instantaneous field of view (IFOV). However, the delineation of rain from wet land surfaces was found to be more difficult.

With the purpose of developing an improved passive microwave technique to delineate rain from wet land surfaces, results from a radiative transfer model suggested using dual polarized multi-frequency

---

[1]Savage, R. C., P. J. Guetter and J. A. Weinman, 1976: The observation of rain clouds over land in Nimbus-6 electrically scanned microwave radiometer (ESMR-6) data. Preprints 7th Conf. Aerospace and Aeronautical Meteorology and Symp. on Remote Sensing from Satellite Melbourne, Amer. Meteor. Soc., 131-136.

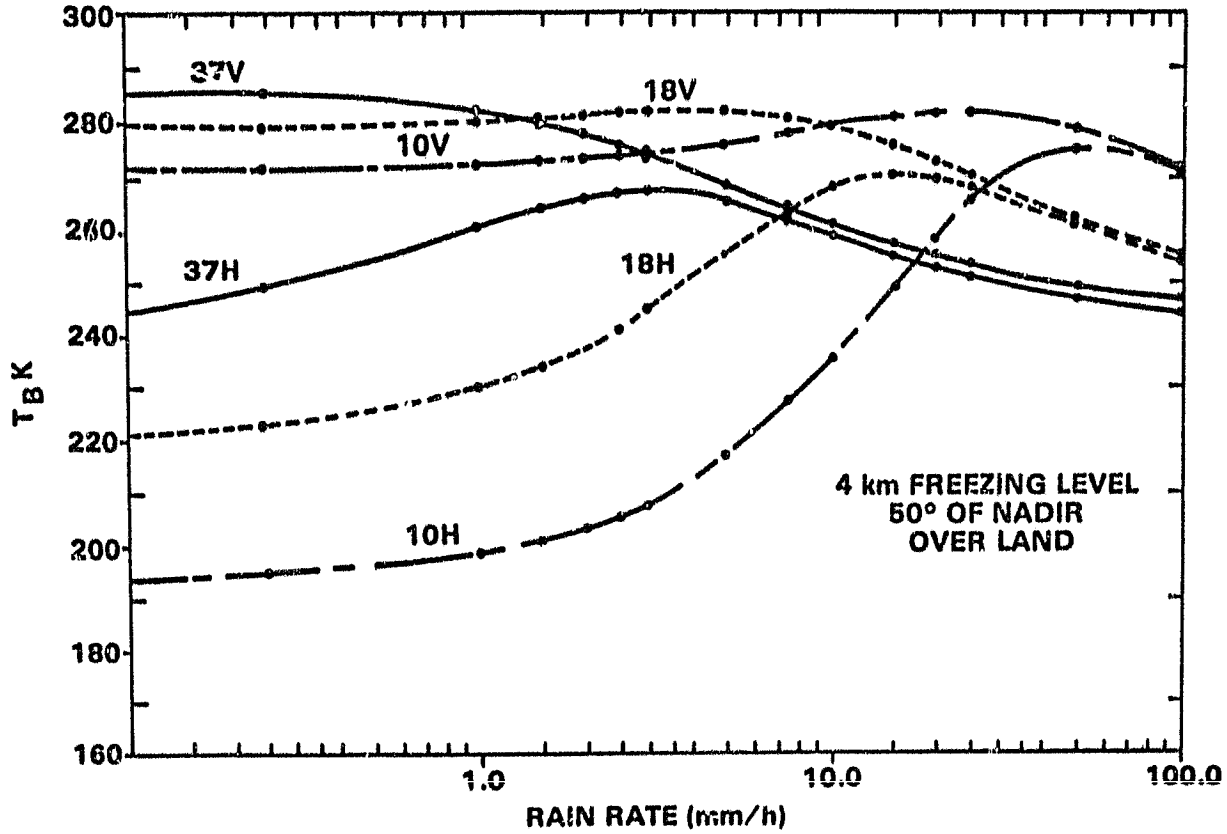

Fig. 1. Rain Rate versus T_B (^oK): Horizontally and vertically polarized brightness temperatures computed at 37.0, 18.0 and 10.7 GHz plotted as a function of rain rate

passive microwave data where the 37 GHz frequency channel data would be augmented by data from the lower frequency channels at 18.0 or 10.7 GHz. These lower frequency channels should have a better capability to differentiate rainfall from land surfaces. This is demonstrated in Fig. 1, which displays the theoretically calculated bipolarized 37.0, 18.0, and 10.7 GHz brightness temperatures (T_B) at 50° incidence angle with the earth surface for a given rain rate. These T_Bs were derived from a radiative transfer model with Lambertial reflection (Born and Wolf, 1975) from land surfaces at a thermodynamic temperature of 299.1K and with a fixed dielectric constant that simulates wet soil of 20% soil moisture content (i.e. a wet ground case) and an atmospheric freezing level at 4 km (Wilheit et al., 1977).

There are several features of interest that the figure delineates. First, the difference between the vertically polarized T_B (T_V) and the horizontally polarized T_B (T_H) becomes less with increasing rain rates; second, the higher the frequency, the more sensitive T_H is to rain (e.g. the highest frequency T_B are affected more by the absorption and reemission and scattering of radiation from rain drops); third, the lower the frequency, the colder the T_B for wet land surfaces with minimum rain rates; and finally, absorption and reemission of radiation from rain drops effects the T_H more than T_V, and the lower the frequency, the larger the warming of T_H for increasing rain rates.

To differentiate rain from wet land surface in the ESMR-6 study (Rodgers et al., 1979) it can be seen from the figure that at rain rates greater than 2 mm h^{-1} the strong backscattering by larger raindrops decreased both T_H and T_V and made the polarization difference small.

However, as delineated by the 37 GHz channel, T_V and T_H curves in the figure the decrease in T_B is small for increasing rain rates. The small dynamic range in T_B for increasing rain rates together with the large ESMR-6 IFOV were the major contributing factors leading to the difficulties in differentiating rain from wet land surfaces. Since rain that was observed with ESMR-6 sometimes did not fill the sensors IFOV, the sensor was observing the partially wet land surface background causing T_B to be warmer and more polarized than would be if the sensor's IFOV was completely filled with rain. These T_B were comparable to the surrounding non-raining wet land surfaces T_B because of the small dynamic range in T_B for increasing rain rates. This problem also occurred when rain rates were too light to attentuate the radiance emitted from the wet land surface background even though the rain completely filled the sensor's IFOV.

To eliminate this problem, the theoretical model suggests that the data from the lower frequency channels should be used to augment the 37 GHz frequency data because of their larger dynamic range in T_H. It is seen in this figure that if rain rates are large enough (where radiance emitted for the rain drops is sufficient to significantly warm the T_H above the non-raining land background (T_H), the greater contrast in T_H at the lower frequencies will improve the delineation of rain from wet land surfaces.

It is the purpose of this study to investigate the application of these ideas with empirical data for the purpose of recommending an improved satellite technique to delineate rain over land. This will be accomplished by statistically analyzing the Nimbus-7 Scanning Multi-channel Microwave Radiometer (SMMR) 37.0, 18.0, and 10.7 GHz data.

This statistical analysis will be performed on each channel by first sampling the T_Bs of the three SMMR channels together with the GOES-1 Visible Infrared Spin Scan Radiometer (VISSR) infrared (11 μm) data for three categories of SMMR T_B's representing rain over land, wet land surface without rain, and dry land surfaces and then testing these populations for uniqueness and separability. A Fisher (1938) linear discriminant classifier will be developed for each SMMR channel and the performance of these algorithms will be checked using an error estimate and with an independent test case. Finally, after considering the results of this study, recommendations will be made concerning a satellite technique that utilizing infrared and dual polarized multifrequency passive microwave data to better detect rain over land.

2. THE SMMR SYSTEM

The SMMR flown aboard Nimbus-7 (Gloersen and Hardis, 1978), which was launched in 1978, measures on alternate days thermal radiation upwelling from the earth's surface and the intervening atmosphere at 5 frequencies, 37.0, 18.0, 21.0, 10.7, and 6.6 GHz. The antenna scans mechanically $\pm$ 25° off nadir every 4 seconds along a conical surface with a vertical axis and a 42° cone angle making a constant incidence angle with the earth's surface of 50°. The instrument measures both horizontal and vertical polarization components for all frequencies. At the four lower frequencies, the radiometers are time shared between the two polarizations, while at 37.0 GHz there are two radiometers, one for each polarization. Because the radiometers for lower frequencies of SMMR are time shared by the vertical and horizontal polarization components, the two polarizations are not viewed simultaneously causing a maximum offset of approximately 28 km between IFOVs with respect to the earth's surface. For the 37.0 GHz channel, the two polarizations are viewed simultaneously. When sampling the lower SMMR frequencies in this study, no attempt was made to correct for this misalignment. The IFOV of the instrument, being proportional to wavelength, ranges from approximately 150 km at 6.6 GHz to 30 km at 37.0 GHz. The data are calibrated using a warm (instrument ambient) and cold (cosmic background) input to the radiometer. The instrument is described in more detail by Gloersen and Barath (1977).

3. DATA SAMPLING

Simultaneous radar measurements of rain and SMMR 37.0, 18.0, and 10.7 GHz T_Bs were needed to sample a given SMMR channel IFOV as rain over land, dry land surfaces, or wet land surfaces. Six daytime synoptic-scale rainfall cases over the eastern and central United States were used where rain data taken from the National Weather Service's WSR-57 radar coincided with the SMMR overpass to within 5 minutes. In two of the cases, the surface thermodynamic temperatures were $\geq$ 15°C, while in the other cases, the thermodynamic temperatures were < 15°C. The cases with the warm surface background had moderate to heavy rain associated with a squall line (30 May 1979) and hurricane David (3 September 1979). Rain areas were sampled within areas delineated as rain by the WSR-57 radar (rain rates $\geq$ 2.5 mm h^{-1}). Wet land surfaces were sampled upwind and adjacent to the rain cells observed on the WSR-57 radar and dry land surfaces were sampled over areas where rain had not fallen within a 24h period previous to the Nimbus-7 pass as determined by surface synoptic maps. The dates and time of the occurrence of these six cases are given in Table 1.

In order to sample the SMMR data, NASA's Atmospheric and Oceanographic Information Processing System (AOIPS) was used to overlay the SMMR and the WSR-57 radar PPI images upon the GOES-1 infrared digital images. A remapping was performed using bilinear interpolation with nearest neighbor resampling and then the AOIPS was used to sample the SMMR data.

An example of the products derived from the remapping program on AOIPS are seen in Figs. 2-7. Figs. 2, 3, and 4 are respectively the

Table 1

Rain Cases

Case	Date	Time GMT
1	20 April 1979	17:30
2	2 May 1979	16:30
3	4 May 1979	17:30
4	30 May 1979	17:43
5	3 September 1979	16:15
6	5 October 1979	16:30

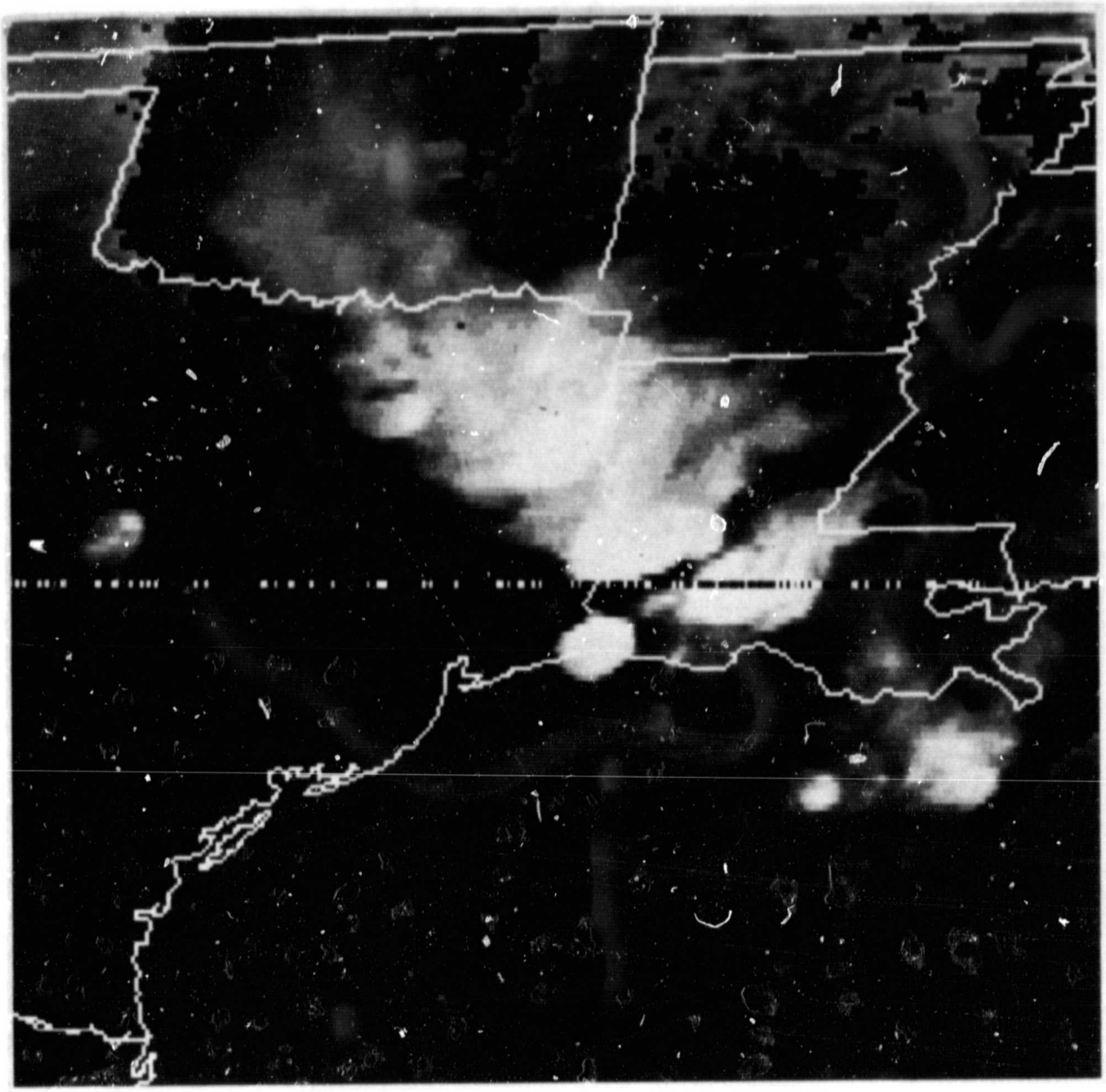

Fig. 2. Lake Charles, LA area, 30 May 1979, remapped GOES-1 IR data: Satellite, IR image of a squall line observed at 17:43 GMT

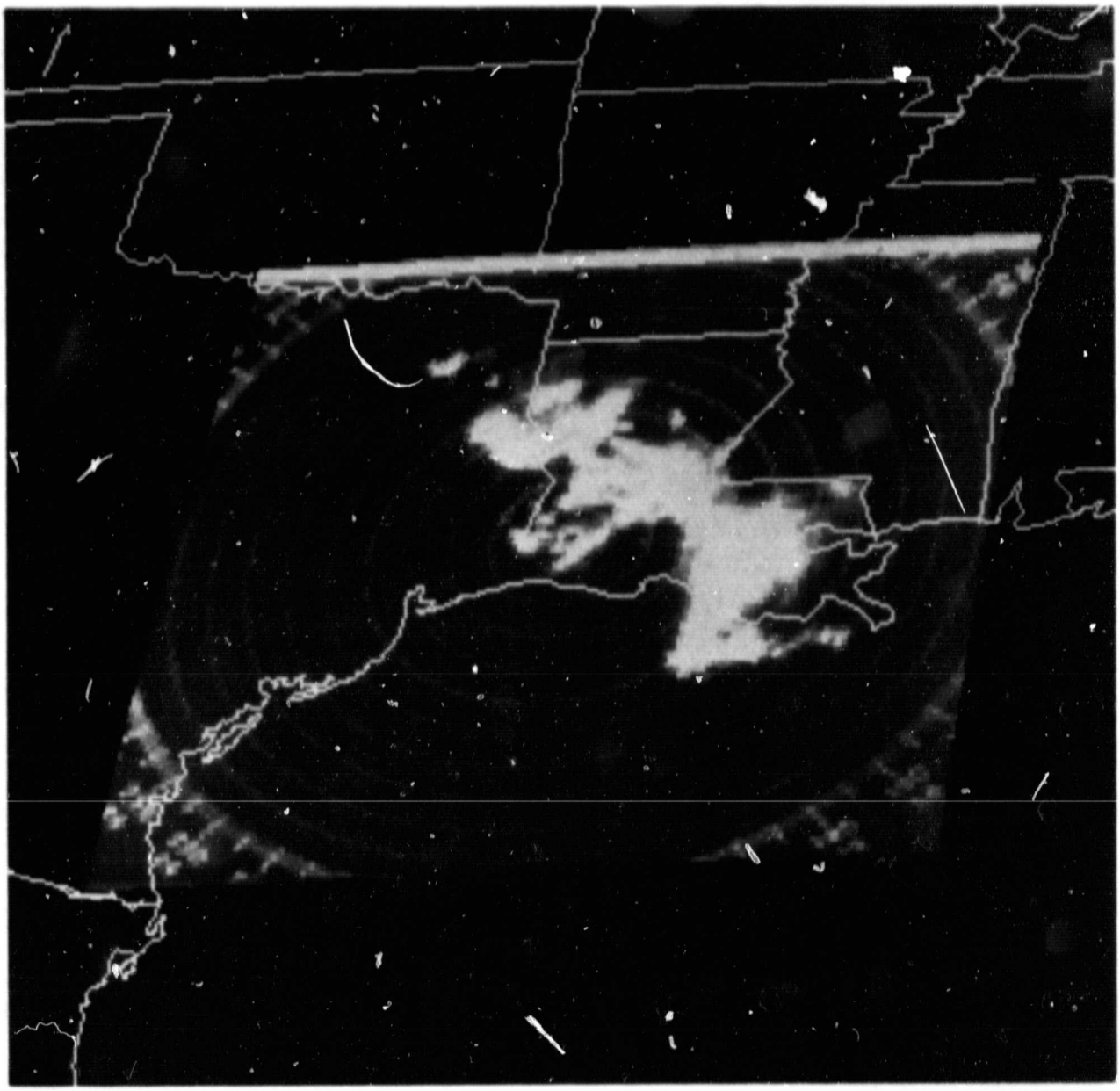

Fig. 3. Lake Charles, LA, 30 May 1979, remapped WSR 57 Radar PPI data: Radar PPI image of a squall line observed at 17:43 GMT from Lake Charles, LA radar. Bright areas represent rain rates exceeding 2.5 mm h^{-1}

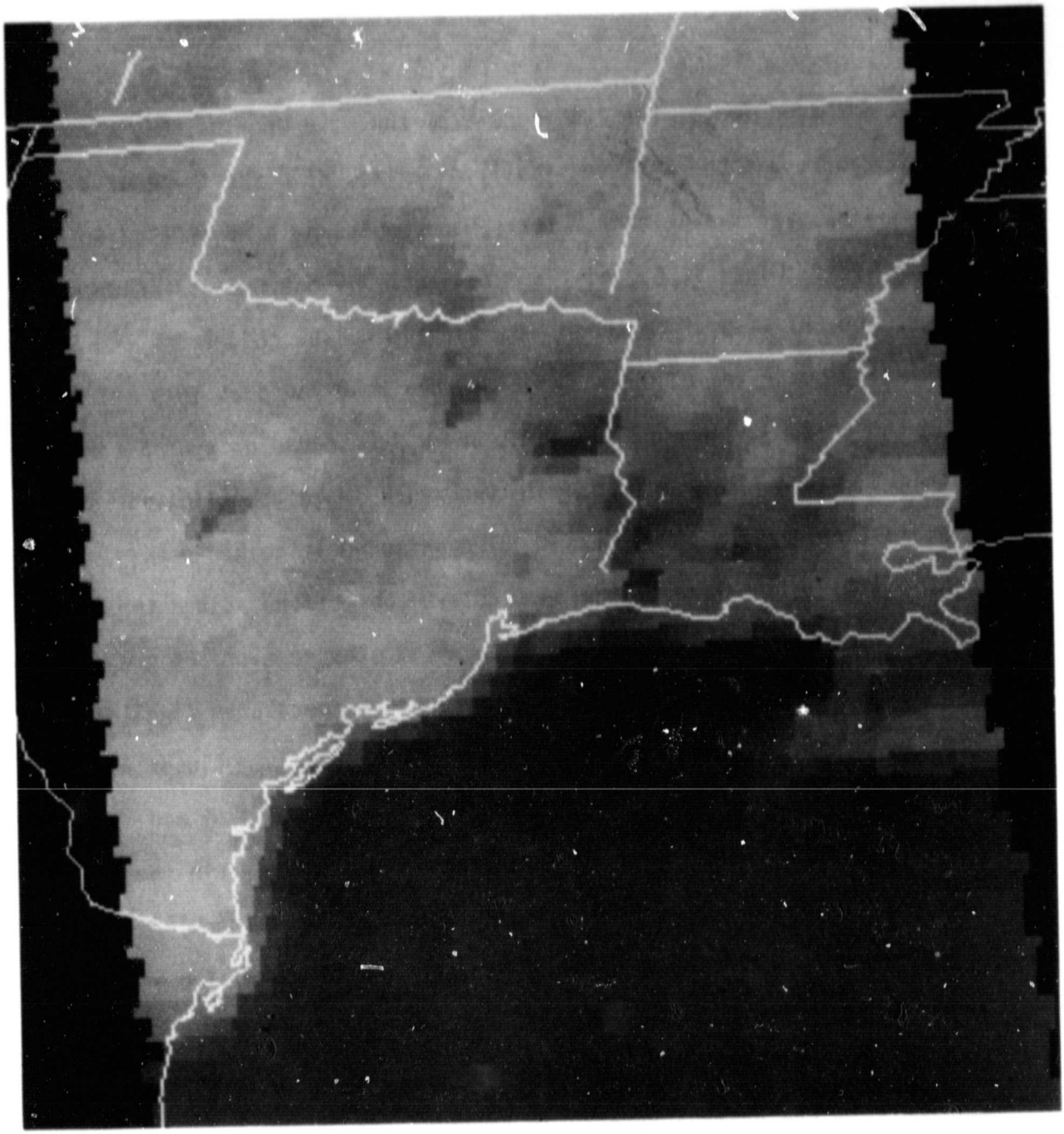

Fig. 4. Lake Charles, LA area, 30 May 1979, remapped Nimbus-7 SMMR vertically polarized 37.0 GHz data: Satellite, vertically polarized 37.0 GHz SMMR image of a squall line observed near 17:43 GMT

GOES-1 infrared image, the PPI image from the Lake Charles, Louisiana WSR-57 radar, and the SMMR vertically polarized 37.0 GHz image of a squall line over the Oklahoma, Texas, and Louisiana area at 1743 GMT on 30 May 1979. Figs. 5, 6, and 7 are respectively the GOES-1 infrared image, the PPI image from the Miami, Florida WSR-57 radar, and the SMMR vertically polarized 37.0 GHz image of hurricane David at 1615 GMT on 3 September 1979. The GOES-1, SMMR, and WSR-57 radar data were taken within 5 minutes of each other. In the radar image, the lightest shades represent rain rates > 2.5 mm h^{-1}. The infrared image has been enhanced to help delineate the most active convection. Cloud tops were shaded into four grey scales (black to white stepped every 64 grey scales) corresponding to equivalent blackbody temperatures (T_{BB}) of 270-240K, 239-220K, 219-210K, and $\leq$ 209K, respectively. Clouds with $T_{BB} \leq 270K$ are probably producing rain (Shenk et al., 1976) and those with $T_{BB} \leq 209K$ are probably producing convective rain (Negri and Adler, 1981). In the SMMR 37 GHz image, the light (dark) shades represent the warmer (colder) T_B. The T_B values from all the SMMR channels are a function of radiance emerging from the earth's surface and the state of the intervening atmosphere. The microwave radiance emitted from the earth's surface is given by εT_S, where ε is the surface emissivity and T_S the surface thermodynamic temperature. The emissivity variation over land is due to the change in the dielectric constant of emitting surface and the biomass. A wet land surface has a larger dielectric constant and, therefore, a lower emissivity. Over water, the emissivity variation is mainly affected by ocean surface roughness. The emissivity varies from $\sim$0.40 over water to

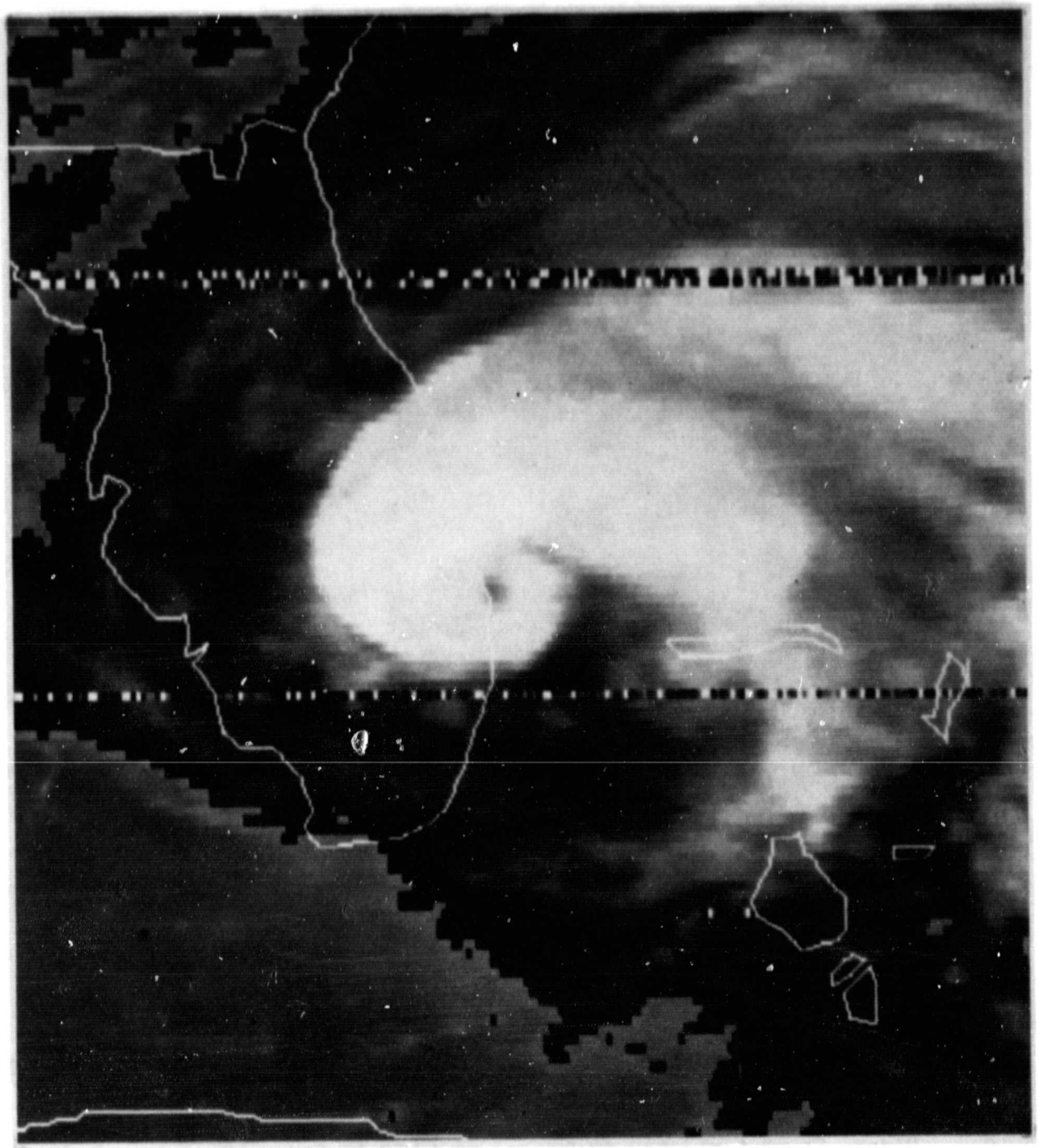

Fig. 5. Miami, FL area, 3 September 1979, remapped GOES-1 IR data: Satellite, IR image of hurricane David observed at 16:15 GMT

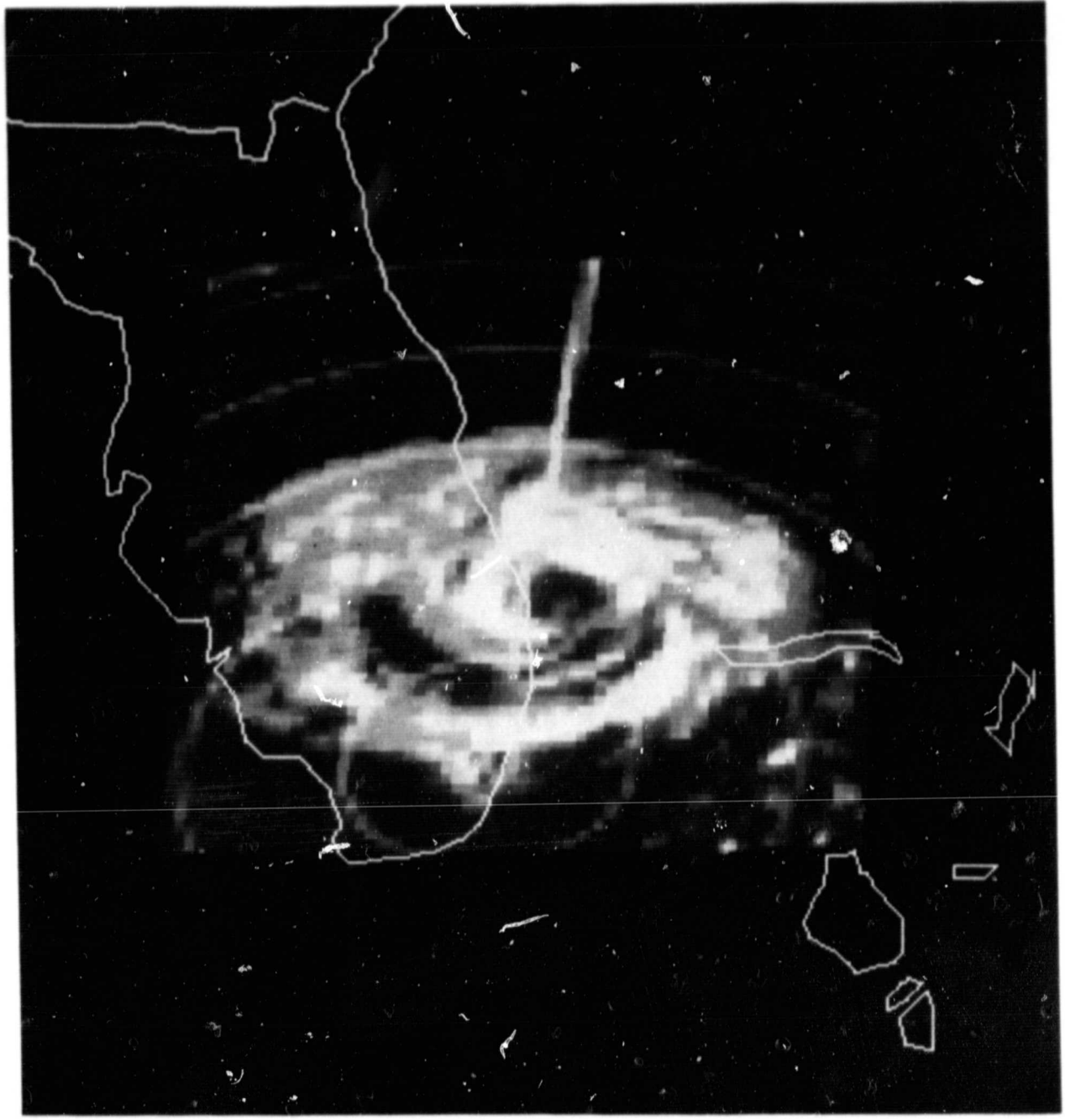

Fig. 6. Miami, FL, 3 September 1979, remapped WSR 57 Radar PPI data: Radar PPI image of hurricane David observed at 16:15 GMT from the Miami, FL radar. The lightest shades represent rain rates of 2.5 mm h^{-1} and white areas represent rain rates exceeding 5.0 mm h^{-1}

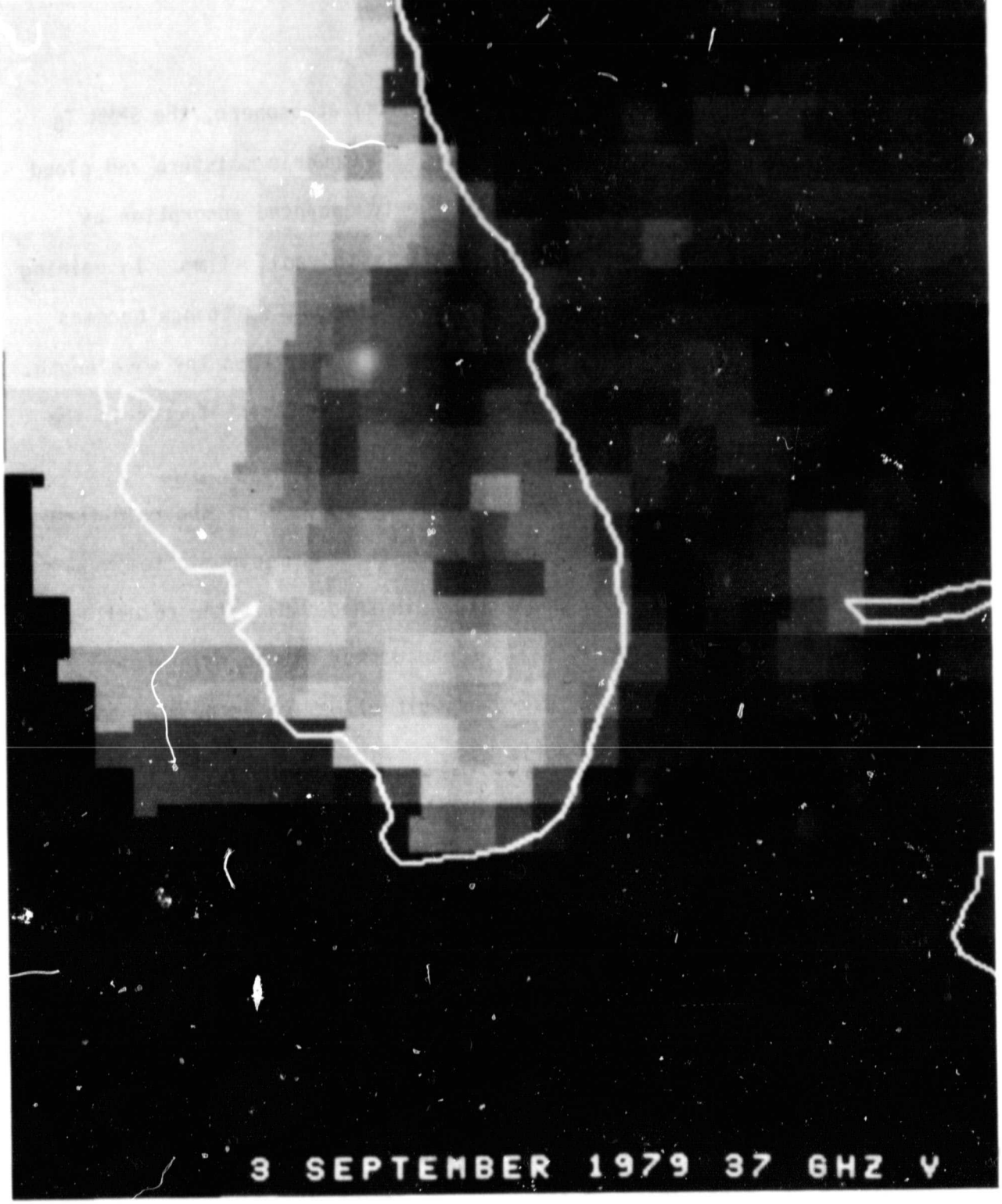

Fig. 7. Miami, Fl area, 3 September 1979, remapped Nimbus-7 SMMR vertically polarized 37.0 GHz data: Satellite, vertically polarized 37.0 GHz SMMR image of hurricane David observed at 16:15 GMT

$\sim$0.95 over dry land. Within the intervening atmosphere, the SMMR T_B is mainly affected by molecular oxygen, atmospheric moisture and cloud liquid water. The greater effect is due to enhanced absorption by liquid water, particularly large droplets with radii >1 mm. In raining clouds where drops are larger than the wavelength, emittance becomes less and scattering greater than for drops smaller than the wavelength. Ice that is found in cirrus clouds is not a significant factor in the SMMR frequency range.

Thus, the warm vertically polarized 37 GHz T_B's of the rain-free dry land areas in these SMMR images where the thermodynamic temperatures are greater than 15°C will appear light in shade while the colder T_B of the rain free ocean areas will appear dark. Within rain areas observed by the WSR-57 radar over the Gulf of Mexico associated with the squall line and over the Atlantic associated with hurricane David the enhanced emission of the radiation by the rain drops causes the T_B's to be warmer (therefore, lighter in shade) than the T_B of the ocean background. Over land, on the other hand, the opposite is true. Due to the large backscattering from the larger rain drops the T_B's are relatively colder than T_B's of the land background.

However, when the land surfaces are wet this contrast is greatly reduced since the T_B are colder due to the decreased emissivity of the background. As mentioned in Section 1, the lack of contrast can also be caused by the combination of the sensor's IFOV not being filled and the small dynamic range in T_B for a given rain rate.

4. STATISTICAL ANALYSIS

Elementary statistics of the sampled SMMR 37.0, 18.0, and 10.7 GHz data from the warm surface background cases are seen in Tables 2, 3, and 4. The tables give for each category the sample size, the mean and standard deviation of the horizontally and vertically polarized T_B, and the correlation and the mean difference between horizontal and vertically polarized T_B's. The SMMR 37.0, 18.0, and 10.7 GHz data for the warm surface case are also shown as scatter plots in Figs. 8, 9, and 10, respectively. In these figures, the C represents the mean of the population and each frequency concentration ellipse encompasses 68% (one standard deviation) of the data within the population. The ellipses reveal the extent of scattering of the data from each population, the correlation between the dual polarization T_B's (T_H and T_V) within each population (the higher the correlation, the larger the eccentricity of the ellipse) and the extent of overlap among the populations. The lines drawn in the figures are the Fisher (1938) linear discriminant lines which separate the rain over land areas (S_R), the dry land surface (S_D), and the wet land surface (S_W) populations represented by the T_B pairs (T_H, T_V) for each SMMR frequency.

It can be seen for the warm surface cases from Tables 2, 3, and 4 and Figs. 8, 9, and 10, that the average T_Bs for the rain areas over land are colder than those from dry land surface areas in all frequencies. However, they are warmer than the wet land surfaces for the 18.0 and 10.7 GHz SMMR channels. Further, the difference between the mean horizontally and vertically polarized T_B's from rain areas over land (wet ground) become progressively smaller (larger) at lower microwave frequencies. It is also seen from the figures that the

Table 2

Elementary Statistics of Sampled 37 GHz
Data: Surface Temperature $\geq 15°C$

	Rain Area		Dry Ground		Wet Soil	
Sample Size: N	71		69		29	
	T_{HR}	T_{VR}	T_{HD}	T_{VD}	T_{HW}	T_{VW}
Mean:	234	256	254	275	234	258
Mean Brightness Temp. Difference	22		21		24	
Standard Deviation: d	7.9	7.7	3.2	2.8	6.7	7.6
Sample Correlation Coefficient Between T_H and T_V: ρ	.96		.97		.88	

Table 3

Elementary Statistics of Sampled 18 GHz
Data: Surface Temperature $\geq$ 15°C

	Rain Area		Dry Ground		Wet Soil	
Sample Size: N	71		69		29	
	T_{HR}	T_{VR}	T_{HD}	T_{VD}	T_{HW}	T_{VW}
Mean:	252	257	264	269	241	
Mean Brightness Temp. Difference	5		5		10	
Standard Deviation: d	4.6	3.7	4.2	2.6	7.1	5.2
Sample Correlation Coefficient Between T_H and T_V: ρ	.59		.66		.80	

Table 4

Elementary Statistics of Sampled 10 GHz
Data: Surface Temperature $\geq 15°C$

	Rain Area	Dry Ground	Wet Soil
Sample Size: N	71	69	29
	T_{HR} T_{VR}	T_{HD} T_{VD}	T_{HW} T_{VW}
Mean:	248 254	260 268	229 244
Mean Brightness Temp. Difference	6	8	15
Standard Deviation: d	9.5 5.3	7.3 5.7	6.8 5.1
Sample Correlation Coefficient Between T_H and T_V: ρ	.86	.65	.44

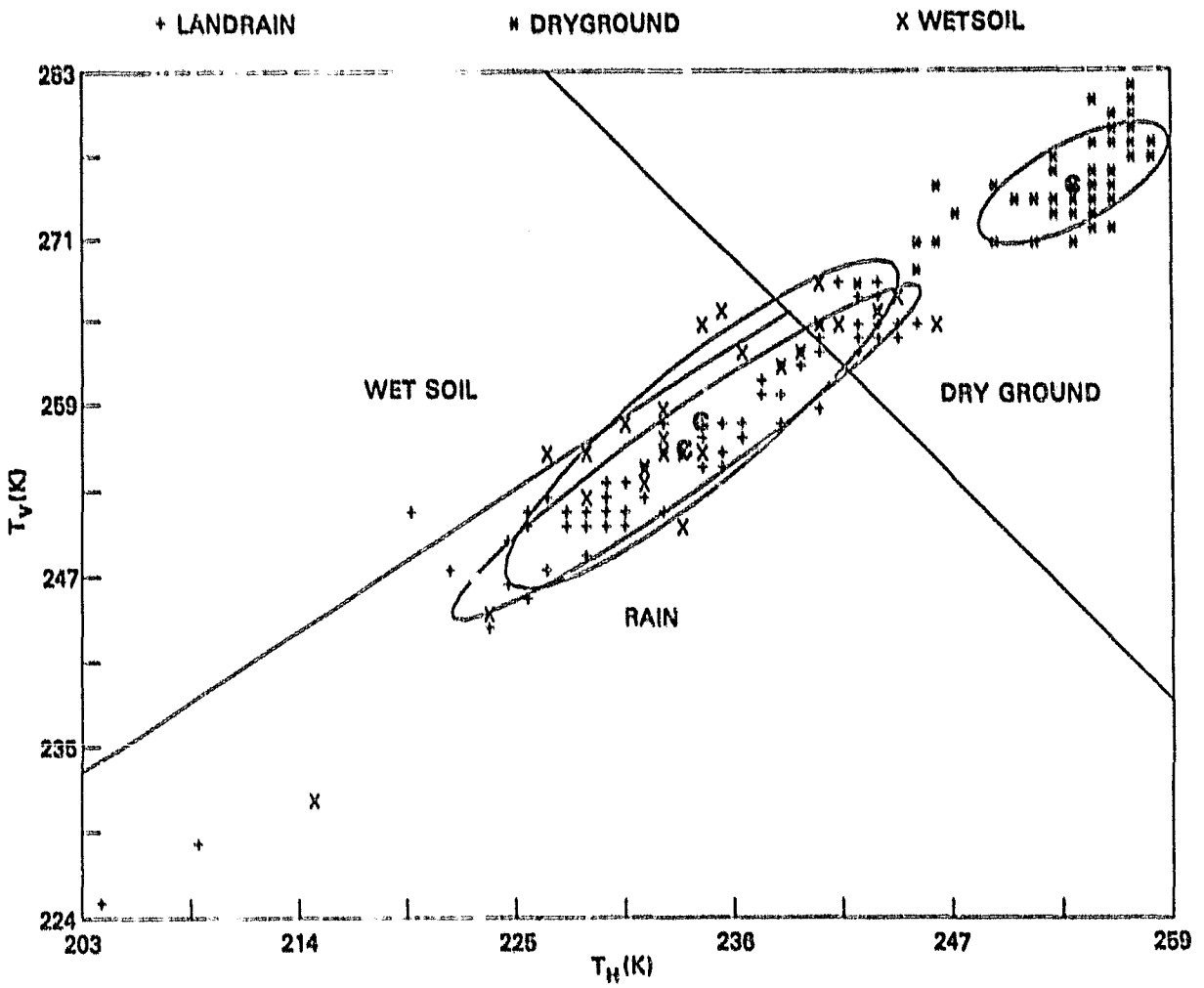

Fig. 8. Nimbus-7 SMMR 37.0 GHz channel scatter-plots for T_H versus T_V: Scatter-plots for each of three sampled category: i.e. rain over land, wet land surfaces, and dry land surfaces.

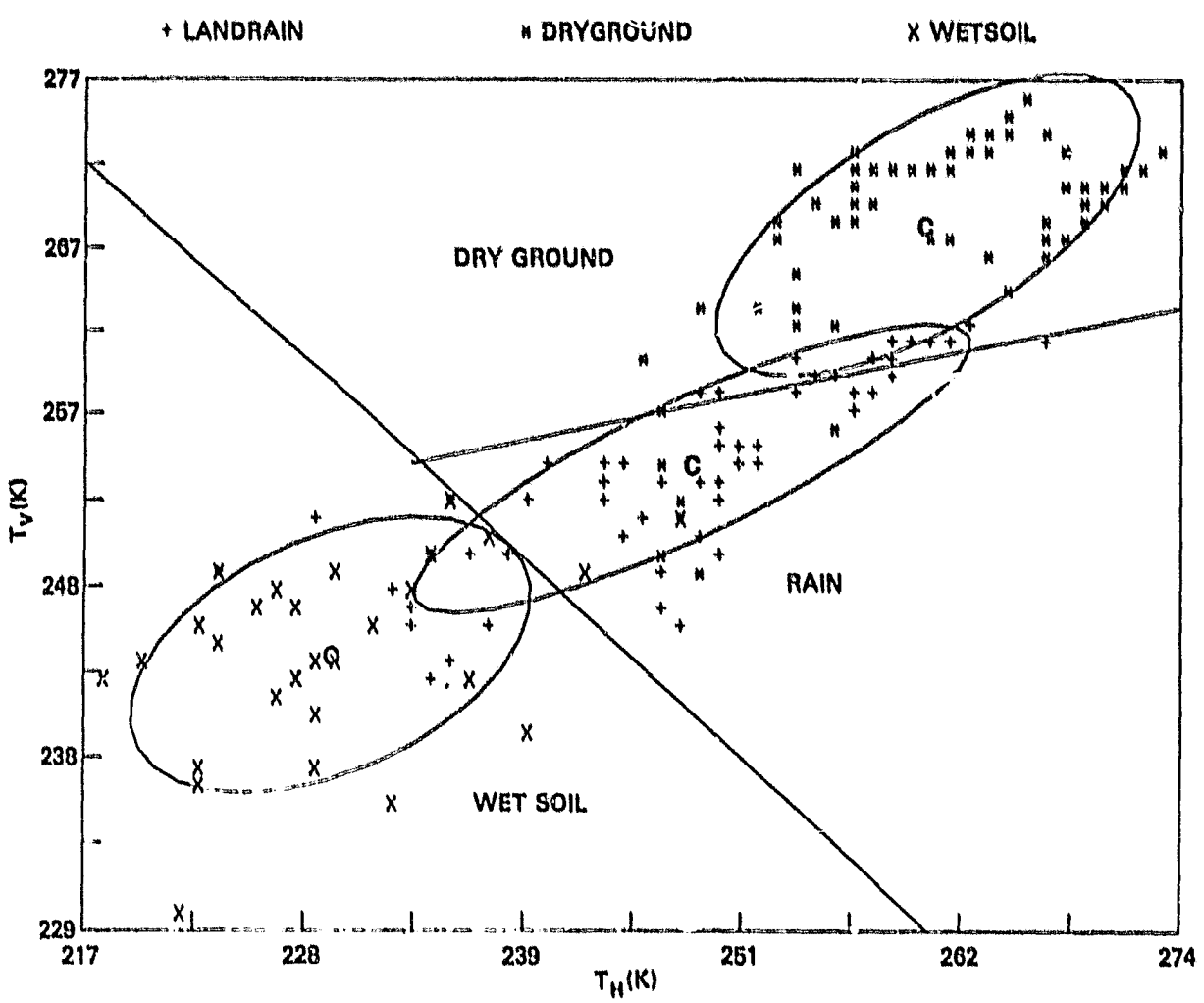

Fig. 9. Nimbus-7 SMMR 18.0 GHz channel scatter-plots for T_H versus T_V: Satellite, vertically polarized 37.0 GHz SMMR image of hurricane David observed at 16:15 GMT

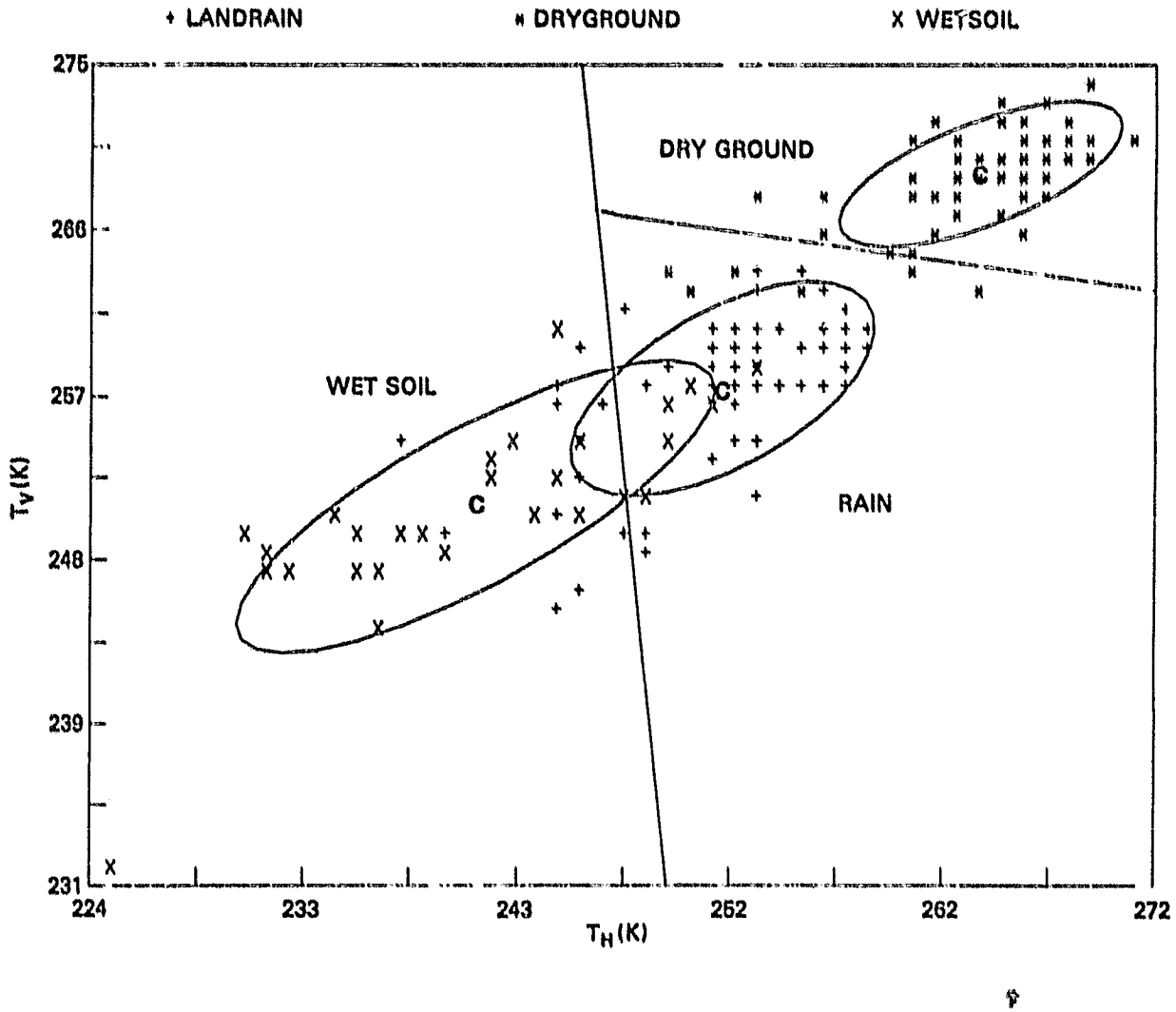

Fig. 10. Nimbus-7 SMMR 10.7 GHz channel scatter-plots for T_H versus T_V: Satellite, vertically polarized 37.0 GHz SMMR image of hurricane David observed at 16:15 GMT

37 GHz channel has the largest overlap of data between wet land surfaces and rain to an even greater extent than found in ESMR-6 data (Rodgers et al., 1979). The reason for this overlap is that sometimes in sampling rain over land, the total upwelling radiance received by the radiometer contains a direct surface contribution. This may occur when the IFOV of the SMMR measurement is partially filled with moderate to heavy rain or when it is completely filled with light rain (background being wet land surface). However, this overlap becomes smaller at lower SMMR frequencies even though the IFOV becomes larger. The decrease of the overlap is attributed to the larger dynamic range of T_H and, therefore, the polarization difference of the lower SMMR frequency between wet ground and moderate and heavy rain over land which is in accordance with the theoretical findings.

In order to verify whether the three populations were statistically distinguishable from one another for the three SMMR channels, a F (variance ratio) test, in terms of Hotellings' T^2 and Mahalanobis' D^2 (Kshirsagar, 1972), was performed to determine the significance of the differences between the means of any two classes. It should be recalled that Mahalanobis' D^2 and Hotellings' T^2 between any two populations are measures of the separability of the two populations. The larger the values of D^2 and T^2, the greater is the separability.

Tables 5, 6, and 7 display D^2 and T^2 as well as the computed and table (critical) value of F for the SMMR 37.0, 18.0, and 10.7 GHz channel data, respectively. All the classes in each frequency except 37 GHz wet ground and rain classes are well separable since computed

Table 5

Significance Between Means (F Test)
SMMR 37 Channel

Between the Means of	Mahalanobis Distance Squared D^2	Hotelling's T^2	The Observed Variance Ratio F	Table Value of F at 1%
Rain and Dry	10	379	188	3.94
Dry and Wet	12	261	129	4.00
Rain and Wet	.163	3.3	1.6	3.99

Table 6

Significance Between Means (F Test)
SMMR 18 GHz Channel

Between the Means of	Mahalanobis Distance Squared D^2	Hotelling's T^2	The Observed Variance Ratio F	Table Value of F at 1%
Rain and Dry	12.67	443.38	220.08	3.94
Dry and Wet	18.62	380.29	118.16	4.00
Rain and Wet	3.33	68.66	33.98	3.99

Table 7

Significance Between Means (F Test)
SMMR 10 GHz Channel

Between the Means of	Mahalanobis Distance Squared D^2	Hotelling's T^2	The Observed Variance Ratio F	Table Value of F at 1%
Rain and Dry	6.48	227.09	112.72	3.94
Dry and Wet	24.38	497.87	246.33	4.00
Rain and Wet	5.46	111.29	55.07	3.99

values for any two populations of each frequency, except the values corresponding to 37 GHz rain and wet ground dta, of D^2 and T^2 are large. Similarly, because the observed value of F is much higher for each pair, than the critical (table) value of F at 1%, the difference between the means of any two classes, except 37 GHz wet land and rain class mean difference, are statistically significant and the chances of any two of these means coinciding is 1 in 100.

Elementary statistics of the sampled 37.0, 18.0, and 10.7 GHz data were also computed for the cold surface background cases. However, since the surface emission is given by εT_S, there should be an influence of the dry land surfaces on T_B. A decrease in T_S results in a decrease in T_B from dry ground and consequently, the T_B contrast between dry land surfaces and rain over land will also decrease at all frequencies. An examination of the 37.0, 18.0, and 10.7 GHz channels for the cold cases (surface thermodynamic temperatures $\leq$15°C), substantiated this effect. As was demonstrated with the ESMR-6 data (Rodgers et al., 1979) for cases whose thermodynamic temperatures were between 5 and 15°C, there was also considerable overlap of the SMMR 37 GHz data between the three populations (figures and tables not shown). This overlap was also observed in the SMMR 18.0 and 10.7 GHz channels. Thus, in the cases where the surface thermodynamic temperatures are $\leq$15°C the lower frequency channel did not help in distinguishing the three populations.

5. CLASSIFICATION ALGORITHM

Since most of the populations for the three channels were found to be statistically distinguishable for only the warm surface case, the Fisher linear discriminant classifier (Fisher 1938) was considered with the purpose of developing a classification algorithm to detect and delineate rainfall over land from dry and wet land surfaces whose thermodynamic temperatures were $\geq$ 15°C, using the SMMR 37.0, 18.0, and 10.7 GHz data.

The purpose of the Fisher linear discriminant classifier is to determine a plane

$$Y = b_0 + b_1 T_H + b_2 T_V$$

which separates two given classes as widely as possible, given the variation of Y within the classes. The desired plane is the one for which b_1 and b_2 are determined by maximizing the function

$$G(b_1, b_2) = \frac{(\bar{Y}_1 - \bar{Y}_2)}{\sum_{i=1}^{2} \sum_{j=1}^{N_i} (Y_{ij} - Y_i)^2} \qquad (2)$$

where Y_1 and Y_2 are the means of Y for the two classes and Y_{ij} is the j^{th} value of Y in the i^{th} class. The constant b_0 is determined so that the discriminant line

$$b_0 + b_1 T_H + b_2 T_V = 0$$

defines the line of separation between the classes. Employing the data for each class and frequency, the following equations of the discriminant lines are determined:

$$L_{RD37} = 9.520 - 0.215\ T_H - 0.016\ T_V = 0 \quad (4)$$

$$L_{RW37} = 1.823 - 0.029\ T_H - 0.033\ T_V = 0 \quad (5)$$

$$L_{RD18} = 17.455 - 0.011\ T - 0.056\ T_V = 0 \quad (6)$$

$$L_{RW18} = 10.6457 - 0.040\ T_H - 0.003\ T_V = 0 \quad (7)$$

$$L_{RD10} = -11.55 - 0.012\ T_H + 0.056\ T_V = 0 \quad (8)$$

$$L_{RW10} = 8.334 - 0.017\ T_H - 0.017\ T_B = 0 \quad (9)$$

where R = Rain areas, D = Dry ground, and W = Wet land. These lines separate the classes S_D, S_R and S_W for the SMMR 37.0, 18.0, and 10.7 GHz channels, as shown in Figs. 8, 9, and 10. Thus, in the Fisher algorithm, the pixel corresponding to a given vector (T_H, T_V) is designated rain over ground, dry ground, or wet soil, respectively, depending on which of the following inequalities are satisfied:

I. 37 GHz Case:

$$L_{RD37}\ (T_H, T_V) < 0 \quad (10)$$

$$L_{RW37}\ (T_H, T_V) < 0 \quad (11)$$

$$L_{RD37}\ (T_H, T_V) > 0 \quad (12)$$

$$L_{RW37}\ (T_H, T_V) > 0 \quad (13)$$

$$L_{RD37}\ (T_H, T_V) < 0 \quad (14)$$

II. 18 GHz Case:

$$L_{RD18}\ (T_H, T_V) > 0 \quad (15)$$

$$L_{RW18}\ (T_H, T_V) < 0 \quad (16)$$

$$L_{RD18}\ (T_H, T_V) < 0 \qquad (17)$$

$$L_{RW18}\ (T_H, T_V) > 0 \qquad (18)$$

$$L_{RD18}\ (T_H, T_V) > 0 \qquad (19)$$

III. 10 GHz Case:

$$L_{RD10}\ (T_H, T_V) < 0 \qquad (20)$$

$$L_{RW10}\ (T_H, T_V) < 0 \qquad (21)$$

$$L_{RD10}\ (T_H, T_V) > 0 \qquad (22)$$

$$L_{RW10}\ (T_H, T_V) > 0 \qquad (23)$$

$$L_{RD18}\ (T_H, T_V) < 0 \qquad (24)$$

Ambiguity will result if any of these strict inequalities become equalities. Test on independent data are described in Section 7.

6. ERROR ANALYSIS

An error estimate was made in order to evaluate quantitatively the performance of the Fisher classification algorithm for the three channels. The error rates were computed according to the asymmetric formulas given by Okamoto (1963). From the results seen in Tables 8, 9, and 10, it is clear that the chance of incorrectly classifying wet land surfaces or dry land surfaces as rain over land is 51% using the 37 GHz channels. However, using the lower frequencies, the errors are greatly reduced (i.e., 23 and 24% for the 18.0 and 10.7 GHz channels, respectively). But when a given SMMR 18.0 or 10.7 GHz pixel is classified as raining area and each of the eight continguous pixels that cluster around it is also classified as rain over land, then the chance of misclassification of that central pixel is reduced to approximately $7.7 \times 10^{-6}\%$ assuming each pixel is independently classified.

Table 8

Probabilities of Misclassification:
Theoretical Computation SMMR
37 GHz Channel

Classified	Rain	Dry	Wet
Rain	49	5	46
Dry	5	91	4
Wet	51	4	45

Average Accuracy: 62 percent

Table 9

Probabilities of Misclassification:
Theoretical Computation SMMR
18 GHz Channel

Classified	Rain	Dry	Wet
Rain	77	4	19
Dry	4	94	2
Wet	19	2	79

Average Accuracy: 83 percent

Table 10

Probabilities of Misclassification:
Theoretical Computation SMMR
10 GHz Channel

Classified	Rain	Dry	Wet
Rain	76	11	13
Dry	11	88	1
Wet	13	1	86

Average Accuracy: 83 percent

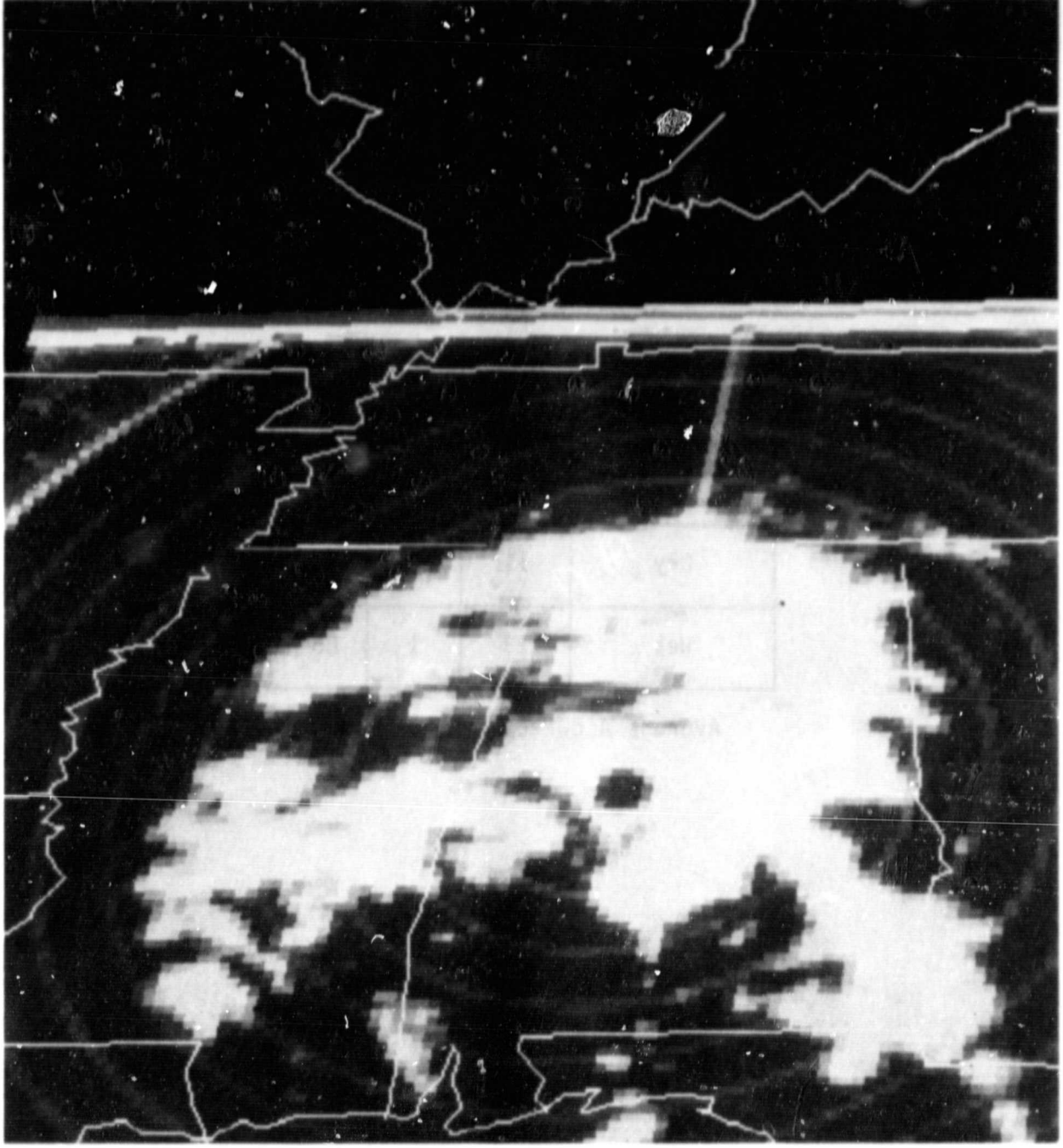

Fig. 11. Centerville, AL, 11 July 1979, remapped WSR 57 Radar PPI data: Radar PPI image of hurricane Bob rain pattern observed at 1700 from the Centerville, AL radar. Bright areas represent rain rates exceeding 2.5 mm h^{-1}

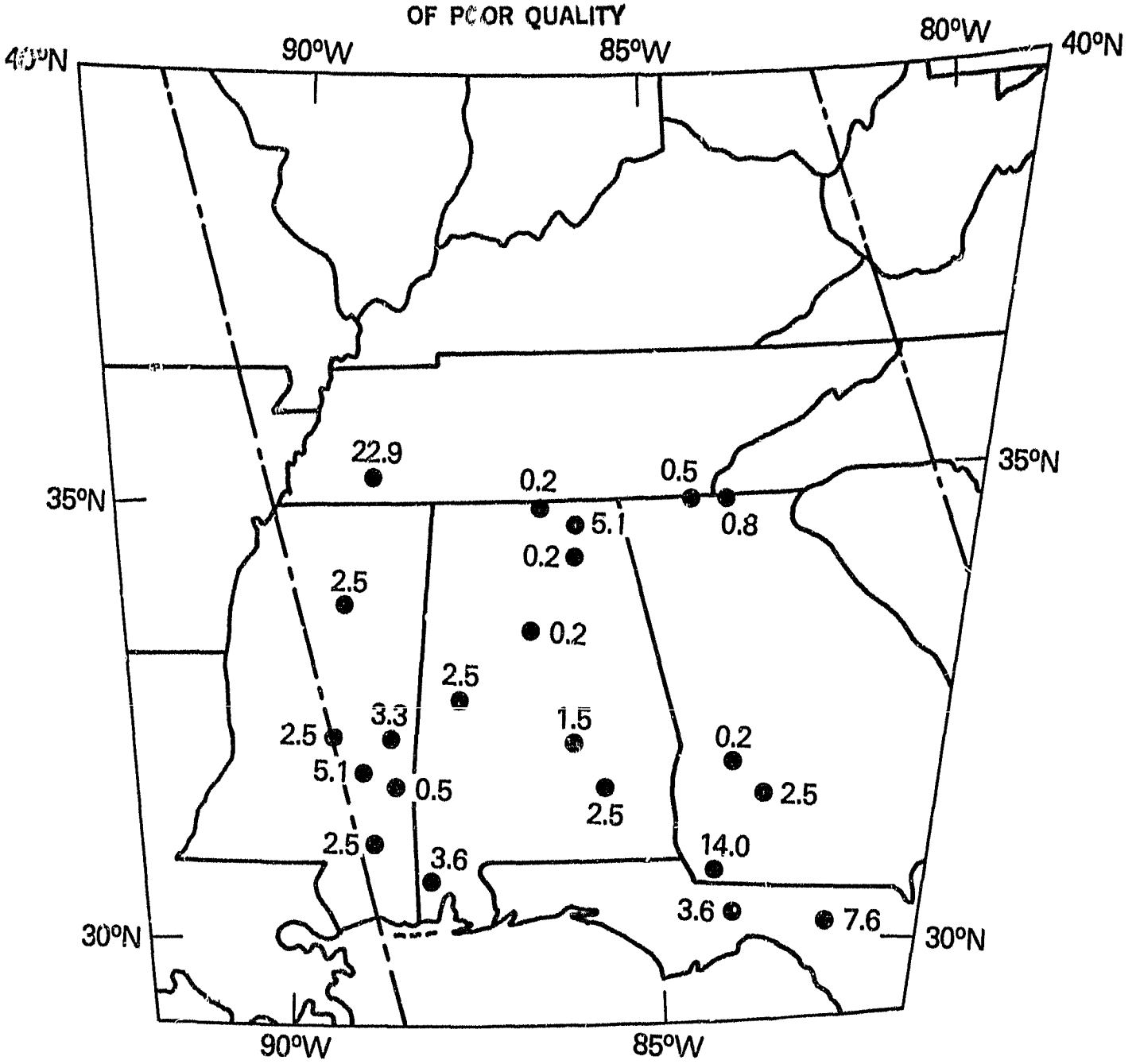

Fig. 12. Centerville, AL area, 11 July 1979, hourly rainfall data: Rainfall amounts associated with hurricane Bob (in mm) for 1600 to 1700 GMT

7. ALGORITHM EVALUATION

To qualitatively verify the performance of the Fisher classification algorithm, a case not previously sampled was tested. This case consisted of a synoptic-scale rain pattern over the southeastern United States associated with hurricane Bob (at approximately 1700 GMT on July 11, 1979) which was observed by the SMMR sensor. The surface thermodynamic temperatures were $\geq$ 15°C. Figs. 11, 12, and 13 show the Centreville, Alabama WSR-57 radar PPI image (white areas delineate rain rates $\geq$ 2.5 mm h^{-1}), hourly rainfall amounts (mm) for the period between 1600 to 1700 GMT, and the storm's cloud top temperatures as measured from GOES-1 VISSR (cloud top temperature enhanced according to the scale mentioned in Section 3), respectively. The approximate times of the radar PPI and GOES-1 infrared measurements were within 5 minutes of the SMMR pass.

The results of the Fisher classification algorithm are seen in Figs. 14, 15, and 16, which show the location of the pixels (located by dots) that were classified as rain over land using the 37.0, 18.0, and 10.7 GHz SMMR channel, respectively. The two lines that encompass the dots are the outer boundaries of the SMMR swath (i.e. $\pm$ 50° of nadir).

It can be seen from Fig. 14 that the 37 GHz T_Bs are doing a surprisingly good job in differentiating the main rain patterns that are delineated by the WSR-57 radar PPI image (Fig. 11). For example, the large rain area in central and northerm Alabama and eastern Mississippi, the rain band through southeastern Alabama and northwestern Florida, and the rain area in southern Tennessee that was only observed by the Nashville, Tennessee (not shown) and ground recording stations (Fig. 12) were very well delineated by the 37 GHz channel.

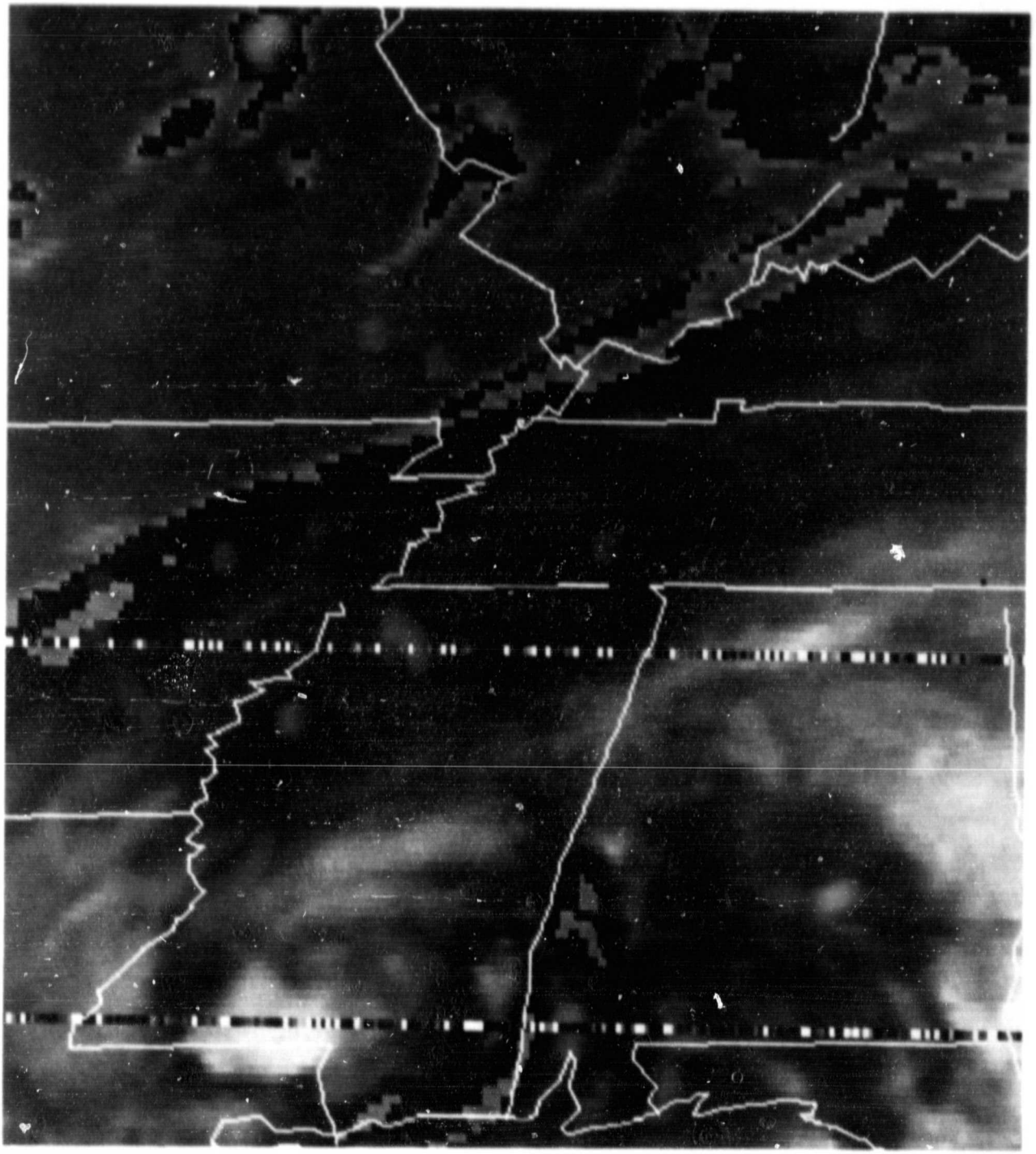

Fig. 13. Centerville, AL area, 11 July 1979, remapped GOES-1 IR data: Satellite IR image of hurricane Bob observed at 1700 GMT

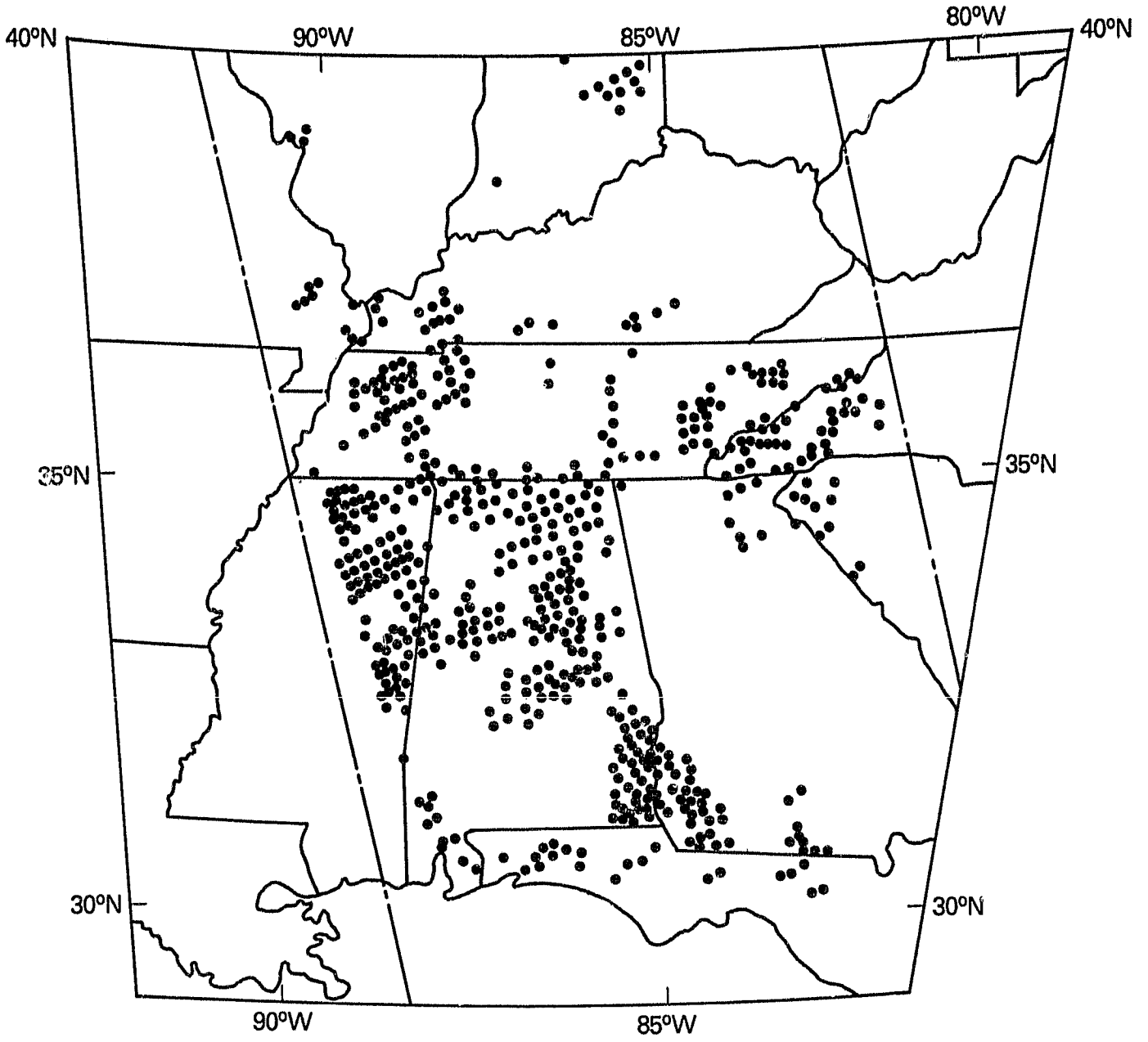

Fig. 14. Centerville, AL area, 11 July 1979, rain locations from Nimbus-7 SMMR 37.0 GHz data: Each dot represents a pixel classified as rain by use of the Fisher classification algorithm

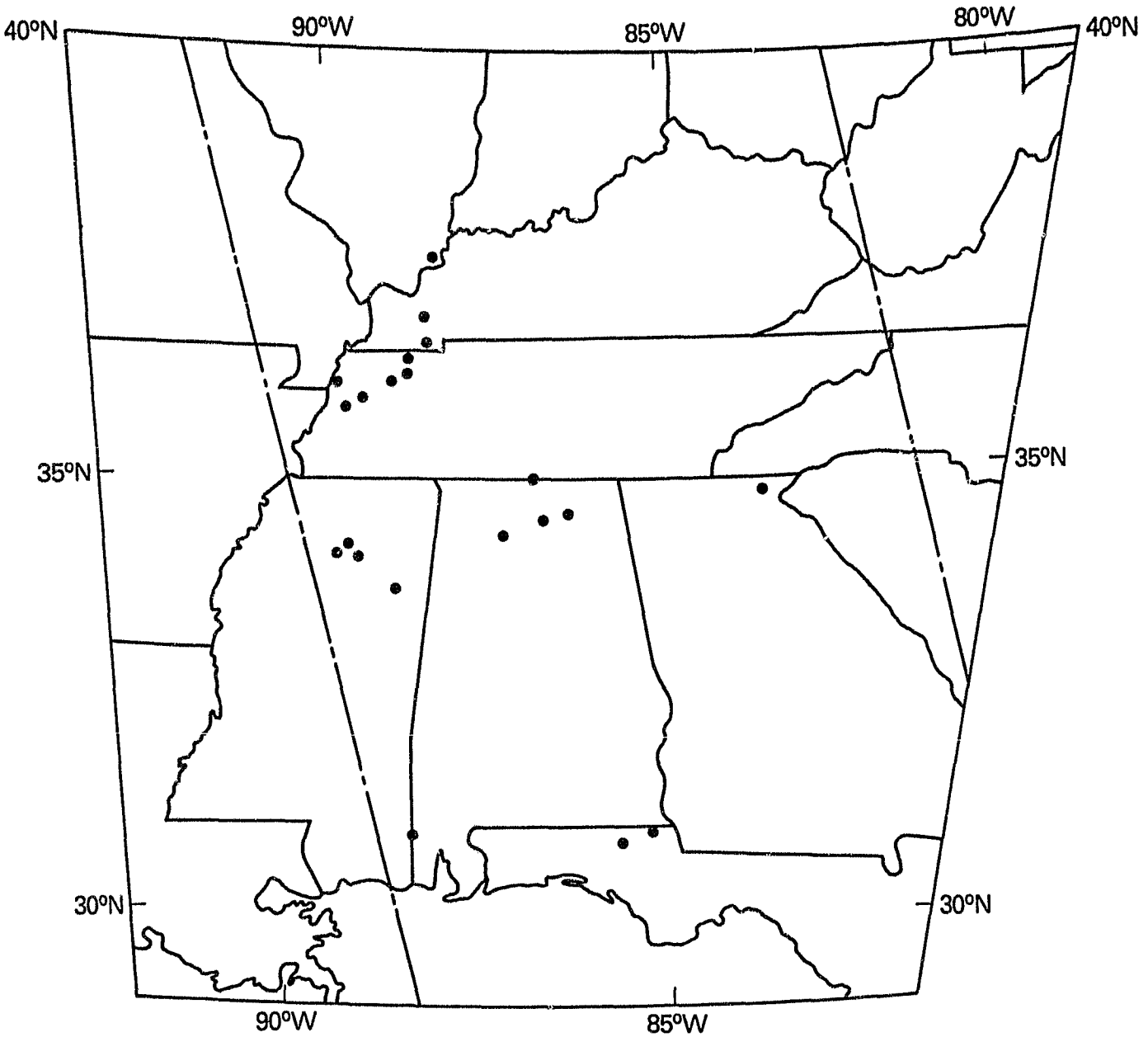

Fig. 15. Centerville, AL area, 11 July 1979, rain locations from Nimbus-7 SMMR 37.0 GHz data: Each dot represents a pixel classified as rain by use of the Fisher classification algorithm

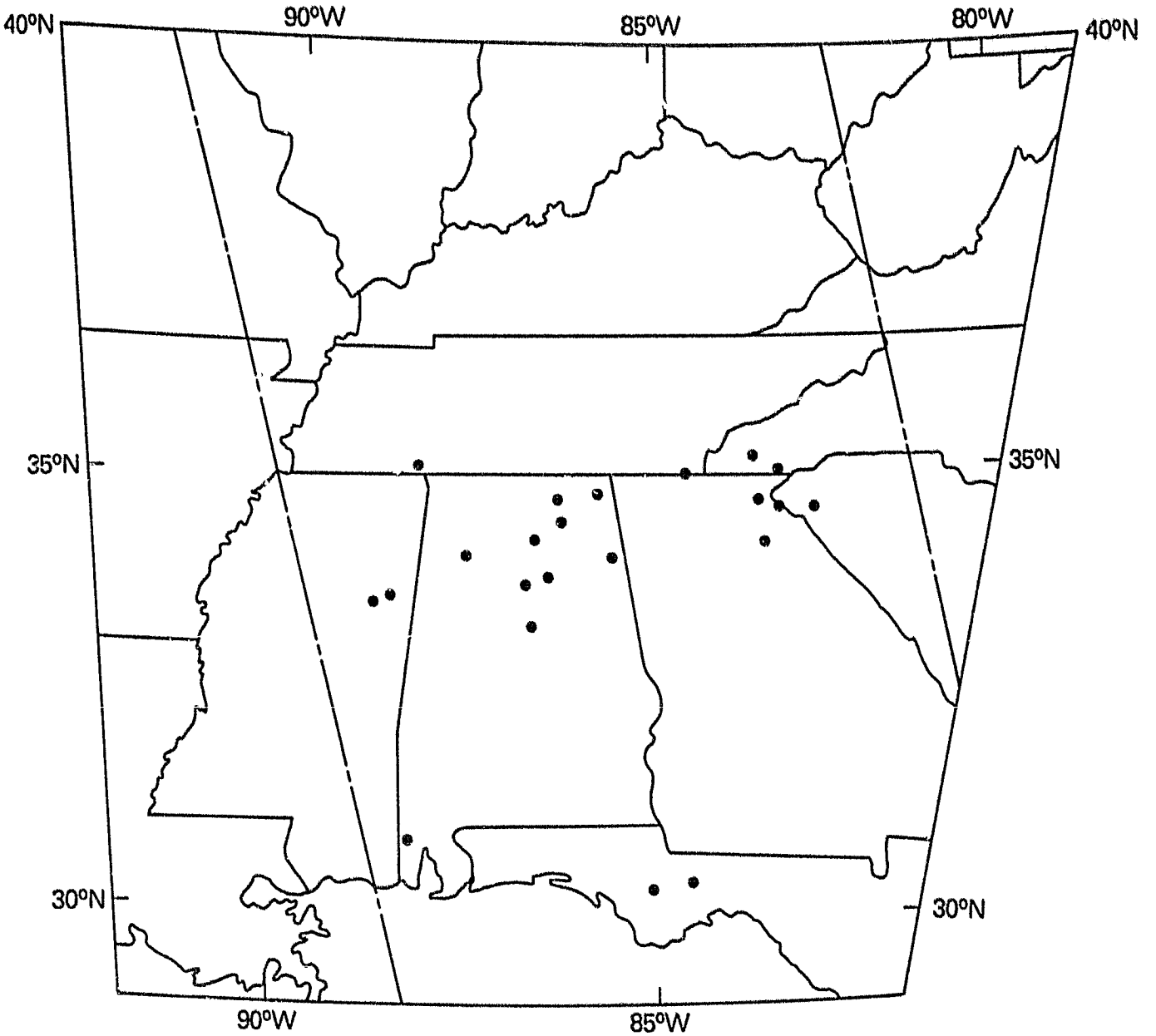

Fig. 16. Centerville, AL area, 11 July 1979, rain locations from Nimbus-7 SMMR 37.0 GHz data: Each dot represents a pixel classified as rain by use of the Fisher classification algorithm

However, there are areas in which the 37 GHz channel depicted rain where rain was not observed. These areas included extreme western Tennessee and Kentucky and southeastern Indiana and parts of western Illinois and eastern Missouri. The majority of these areas except Illinois and Missouri, were cloudy with cloud top $T_{BB} < 270$ (see Fig. 12). The misclassification in the majority of these areas was caused by rivers, lakes, and adjacent wet ground, such as the Mississippi River in southern Illinois and lakes Barkley and Kentucky in western Kentucky. The reason for the misclassification in the other areas is also probably caused by wet land surfaces.

Examining the Fisher algorithm developed from the 18.0 and 10.7 GHz SMMR T_Bs (Figs. 15 and 16, respectively) it is seen that very few pixels are classified as rain as compared to the algorithm developed from the 37 GHz data. This is because the lower frequency SMMR channels are less sensitive to rain (see Fig. 1). However, if the rain rates are great enough and fill the sensor's IFOV, the chances of misclassification rain over land have been shown theoretically and observationally to be less than with the 37.0 GHz channel due to the large dynamic range in T_H for increasing rain rates.

Comparing the Fisher algorithms developed from the 18.0 and 10.7 GHz SMMR T_Bs (Figs. 15 and 16, respectively) with the Centreville, Alabama WSR-57 radar PPI image (Fig. 11) it appears that the majority of the pixels that are classified as rain are located in areas of rain as depicted by the radar. Further, when the Fisher algorithm is compared with the hourly rainfall amounts between 1600 and 1700 GMT (Fig. 12) it also appears that the majority of the stations recording rainfall amounts greater than 1 mm during the hour are located

within the cluster of pixels that have been classified as rain in both channels. Heavy rain amounts measured by the ground stations in southeastern Mississippi were not classified as rain since these pixels were near the edge of the SMMR swath. The pixels that were classified as rain in northern Georgia, western North Carolina and eastern Tennessee had rain rates less than 1 mm h^{-1} during the hour according to the reporting stations. However, because of the orography in this area, these recorded rainfall amounts may not be representative of the rain rates that would be observed by SMMR.

The major discrepancy found with these two algorithms was with the algorithm developed with the 18.0 GHz data. The misclassified pixels were located in western Kentucky and northern Tennessee and again may be caused by the wet land surfaces associated with the Mississippi River and lakes Barkley and Kentucky. However, it can be seen in Fig. 16 that the algorithm developed from the SMMR 10.7 GHz T_B did not misclassify these pixels. This indicates that if the rain rates are heavy enough and fill the sensors IFOV, the 10.7 GHz channel would be the best of the three channels to differentiate rain from wet ground.

8. CONCLUSIONS AND RECOMMENDATIONS

A statistical analysis was performed on the Nimbus-7 SMMR dual polarized 37.0, 18.0, and 10.7 GHz data with the purpose of assessing whether the 18.0 and 10.7 GHz channels could reduce the ambiguities found in using the 37.0 GHz radiometer data to differentiate rain areas from wet land surfaces. Results from the F test of the data showed that neither of the SMMR channels could differentiate rain from wet or dry land when surface thermodynamic temperatures were less than 15°C. However, when the surface thermodynamic temperatures were $\geq$ 15°C, the F test indicated that the probability that the mean vectors of any two populations being identical was less than .01 except for the rain over land and wet ground class observed with the SMMR 37 GHz channel. An error analysis of the SMMR data for the warm land surface cases revealed that the 37.0 GHz channel could only correctly classify rain or wet land from dry land while the lower frequency SMMR channels could accurately classify rain from both dry and wet land surfaces provided that the rain rates were large enough and sufficiently filled the sensor's IFOV so that the T_H was affected. An independent testing of the Fisher classification algorithms developed for each of the three SMMR channels further substantiated these findings. For example, there were areas which were misclassified as rain by the 37 GHz channel, but were correctly classified by the lower frequency SMMR channels.

Thus, it appears that the lower frequency channels will better differentiate rain over dry or wet land surfaces. However, because the SMMR channels are less sensitive to rain and have a larger IFOV, areas of light rain or rain that occurred over small areas would not be observed. As was observed in the independent test case, the 37 GHz

channel did surprisingly well in delineating rain when compared to the radar in the cloudy areas whose cloud top T_{BB} was <270K, inspite of areas of misclassification. Therefore, the study suggests that the ability to observe rain over land decreases with decreasing SMMR frequency, but when rain is observed at these lower frequencies, the degree of confidence increases in delineating rain over land. In light of the results of this study and the ESMR-6 study (Rodgers et al., 1979), an improved rain over land detection technique could be developed that utilizes both the satellite infrared and multi-frequency dual polarized passive microwave data. Fig. 17 displays a flow diagram that describes such a technique. The flow diagram shows the following: 1) The determination of the surface thermodynamic temperatures could be obtained from either surface meteorological data or from satellite infrared data in cloud free areas; 2) In areas where $T_{sfc} \geq 15°C$, the presence of possible raining clouds could be detected again using satellite infrared data. Shenk et al., (1976) suggested that clouds that are probably producing rain have cloud top $T_{BB} < 270K$; 3) To eliminate the problem of misclassification caused by dew at night using the passive microwave data (Rodgers et al., 1979), the dew point depression obtained from the surface stations would be examined if available. However, the chances of dew occuring in cloudy conditions at night is less likely than during cloud free periods. A classification of rain by the 37 GHz SMMR data in clear regions at night would indicate either wet land or dew. If dew was indicated in the cloudy regions, the passive microwave data would not be able to differentiate rain from dew;

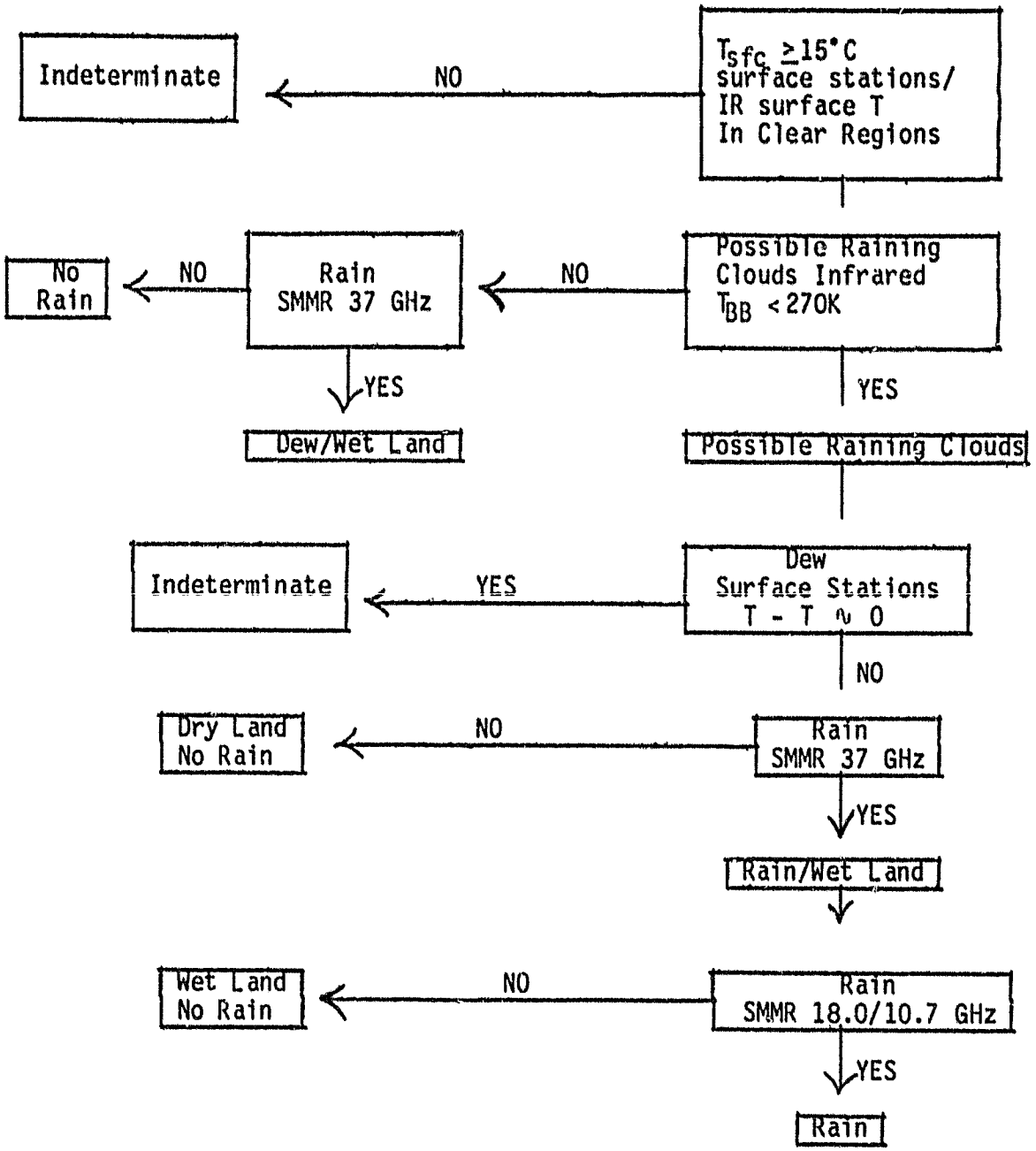

Figure 17. Infrared/Passive Microwave Technique To Delineate Rain Over Land

4) In the cloudy regions whose cloud top T_{BB} are less than 270K, the SMMR 37 GHz data would be used to differentiate rain and wet land from dry land; 5) Within these areas delineated as rain and/or wet land by the SMMR 37.0 GHz channels, the 18.0 and 10.7 GHz channels would be used to improve the degree of confidence that rain was being observed by the 37.0 GHz channel.

REFERENCES

Born, M., and E. Wolt, 1975: Principles of Optics. Pergamon Press, 182 pp.

Fisher, R. A., 1938: The statistical utilization of multiple measurements. Ann. Eugenics, 8, 276-386.

Gloerson, P. and F. T. Barath, 1977: A scanning multichannel microwave radiometer for Nimbus-6 and Seasat-A. IEE J. Ocean Eng'g., OE-2, 172-178.

_____, Hardis, L., 1978: The scanning multichannel microwave radiometer (SMMR) experiment. Nimbus-7 User's Guide. NASA Goddard Space Flight Center, 213-245.

Kshirsagar, A. M., 1972: Multivariate Analysis. Marcel Dekker, 534 pp.

Negri, A. J., and R. F. Adler, 1981: Relation of Satellite-Based Thunderstorm Intensity to Radar-Estimated Rainfall. J. Appl. Meteor., 20, 282-300.

Okamoto, M., 1963: An asymptotic expansion for the distribution of the linear discriminant function. Ann. Math. Statist., 34, 1286-1301.

Rodgers, E. B., H. Siddalingaiah, A.T.C. Chang, and T. Wilheit, 1979: A statistical technique for determining rainfall over land employing Nimbus-6 ESMR measurements J. Appl. Meteor., 18, 978-991.

Savage, R. C., and J. A. Weinman, 1975: Preliminary calculations of the upwelling radiance from rain clouds at 37.0 and 19.35 GHz. Bull. Amer. Meteor. Soc., 56, 1272-1274.

Savage, R. C., and P. J. Guetter and J. A. Weinman, 1976: The observation of rain clouds over land in Nimbus-6 electrically scanned microwave radiometer (ESMR-6) data. Preprints 7th Conf. Aerospace and Aeronautical Meteorology and Symp. on Remote Sensing from Satellite, Melbourne, Amer. Meteor. Soc., 131-136.

Shenk, W. E., R. J. Holub, and R. A. Neff, 1976: A multispectral cloud type identification method developed for tropical ocean areas with Nimbus-3 MRIR measurements. Mon. Wea. Rev., 104, 284-291.

Weinman, J. A., and P. J. Guetter, 1977: Determination of rainfall distribution from microwave radiation measured by the Nimbus-6 ESMR. J. Appl. Meteor., 16, 437-442.

Wilheit, T. T., A.T.C. Chang, M.S.V. Rao, E. B. Rodgers and J. S. Theon, 1977: A satellite technique for quantitatively mapping rainfall rates over the oceans. J. Appl. Meteor., 16, 551-560.